Structural Variation Induced by Different Nucleotides at the Cleavage Site of the Hammerhead Ribozyme†

Jean-Pierre Simorre,[‡,§] Pascale Legault,[‡,||] Narayan Baidya,[‡,⊥] Olke C. Uhlenbeck,[‡] Lara Maloney,[#] Francine Wincott,[#] Nassim Usman,[#] Leonid Beigelman,[#] and Arthur Pardi*[,‡]

Department of Chemistry and Biochemistry, University of Colorado, Boulder, Boulder, Colorado 80309-0215, and Ribozyme Pharmaceuticals Inc., 2950 Wilderness Pl., Boulder, Colorado 80301

Received October 8, 1997; Revised Manuscript Received January 5, 1998

ABSTRACT: The hammerhead ribozyme is capable of cleaving RNA substrates at 5′ UX 3′ sequences (where the cleavage site, X, can be A, C, or U). Hammerhead complexes containing dC, dA, dI, or rG nucleotides at the cleavage site have been studied by NMR. The rG at the cleavage site forms a Watson−Crick base pair with C3 in the conserved core of the hammerhead, indicating that rG substrates inhibit the cleavage reaction by stabilizing an inactive conformation of the molecule. Isotope-edited NMR experiments on the hammerhead complexes show that there are different short proton−proton distances between neighboring residues depending upon whether there is a dC or dA at the cleavage site. These NMR data demonstrate that there are significant differences in the structure and/or dynamics of the active-site residues in these hammerhead complexes. Molecular dynamics calculations were used to model the conformations of the cleavage-site variants consistent with the NMR data. The solution conformations of the hammerhead ribozyme−substrate complexes are compared with the X-ray structure of the hammerhead ribozyme and are used to help understand the thermodynamic and kinetic differences among the cleavage-site variants.

The hammerhead ribozyme consists of a small conserved core sequence surrounding three branched helical regions (*1, 2*). In the presence of various divalent ions, the hammerhead ribozyme cleaves a specific phosphodiester bond to yield a 2′,3′ cyclic phosphate and a 5′ OH (*3, 4*). Two X-ray crystal structures of hammerhead ribozyme−substrate complexes were independently determined using different constructs, and the conformation of the catalytic core is the same in both structures (*5, 6*). These structures were performed on a complex of a ribozyme with noncleavable substrate complexes containing either a dC or 2′ O-methyl C at the cleavage site. In the X-ray structures, the cytosine at the cleavage site (C17) forms a single hydrogen-bonded base pair with residue C3 in the catalytic core (*5, 6*). The catalytic activity of the hammerhead is very similar whether there is a C, A, or U at the cleavage site (*2, 7*−*13*). Therefore, some rearrangement at the active site must take place to accommodate different nucleotides at the cleavage site. In addition, there are other indications that, for catalysis to occur, there are structural changes or dynamics at active site. The hammerhead reaction is thought to require in-line attack of the cleavable phosphate with the 2′ OH of the nucleotide at the cleavage site (*10, 14, 15*); however, the conformation in the X-ray structures does not allow for in-line attack. Thus, various models have been proposed for how the conformation in the X-ray structure changes to proceed through the transition state (*5, 6, 16*−*18*).

To probe the structural variations induced by having different bases at the cleavage site, we have performed NMR structural studies on the hammerhead ribozyme with substrates having different nucleotides at the cleavage site. It was previously hypothesized that a G17 at the cleavage site forms a base pair with residue C3 in the catalytic core which inhibits cleavage (*2, 10, 19*). The NMR results obtained here demonstrate formation of this G17−C3 Watson−Crick base pair, confirming that at least part of the lower cleavage rate of the G substrate results from stabilization of an inactive conformation. The NMR structural data for hammerhead complexes containing dA and dC substrates also demonstrate that there are significant differences in the structure and/or dynamics of the active site in these two hammerhead complexes. These structural data are used in conjunction with the X-ray structures to model conformational changes that occur when different bases occupy the cleavage site. These NMR and modeling studies are used to help understand differences in the kinetic and thermodynamic parameters for cleavage-site variants in the hammerhead ribozyme.

† This work was supported by NIH Grant AI30726 and a Research Career Development Award AI01051 to A.P., a NATO/CNRS Fellowship to J.P.S., a NSERC 1967 Science and Engineering scholarship and a FCAR scholarship to P.L., a Damon Runyan−Walter Winchell Postdoctoral Fellowship (DRG 1280) to N.B. and NIH Grant GM36944 to O.C.U. We also thank the Colorado RNA Center for support of RNA research on the Boulder campus.

* To whom correspondence should be addressed.

‡ University of Colorado.

§ Present address: Institut de Biologie Structurale, CEA-CNRS, 41 Avenue des Martyrs, F-38027 Grenoble Cedex, France.

|| Present address: Department of Molecular and Medical Genetics, One King's College Circle, University of Toronto, Toronto, Ontario, M5S 1A8, Canada.

⊥ Present address: Hyseq Inc., 670 Almonaro Ave., Sunnyvale, CA 94086.

Ribozyme Pharmaceuticals Inc.

S0006-2960(97)02493-8 CCC: $15.00
Published on Web 03/03/1998

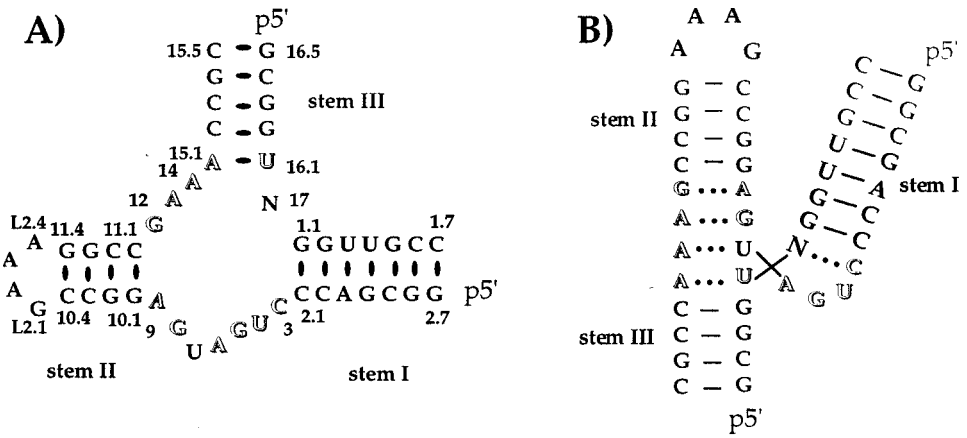

FIGURE 1: (A) The sequence and secondary structure of the hammerhead ribozyme R19−substrate S19N17 complex is shown. (B) An alternate representation of the hammerhead which reflects the conformation observed in the X-ray crystal structures (*5*, *6*). The R19 ribozyme and S19N17 substrate are 34 nucleotides and 13 nucleotides long, respectively. N17 refers to the nucleotide at the cleavage site and substrates containing dA17, dC17, rG17, and dI17 were studied. The conserved catalytic core is indicated by outlined characters (*1*, *2*), and the standard numbering system for the hammerhead ribozyme is shown (*40*).

MATERIALS AND METHODS

Preparation of the RNA Molecules. The sequences for the R19 hammerhead ribozyme and the S19 substrates are shown in Figure 1. Four different ribozyme−substrate complexes were studied where the nucleotide at the cleavage site was a dA, dC, dI, or rG and these substrates will be referred to as S19dA17, S19dC17, S19dI17, and S19G17, respectively. For S19dA17, S19dC17, and S19dI17, all residues are ribose sugars except for a deoxyribose at the cleavage site, whereas all residues are ribose sugars in S19G17. The substrates were chemically synthesized and purified as previously described (*20*, *21*) with S19G17 and S19dI17 purified by electrophoresis on 20% polyacrylamide gels and S19dA17 and S19dC17 purified by HPLC using anion exchange and/or reversed-phase C-18 columns. The substrates were desalted on a DEAE-Sephacel column. The unlabeled R19 and $^{13}C/^{15}N$-labeled R19 ribozymes were prepared by in vitro transcription with T7 RNA polymerase and purified as previously described (*22*, *23*), except for the R19 in the unlabeled R19:S19dC17 complex which was chemically synthesized.

The R19 ribozyme samples were dialyzed extensively against buffer containing 25 mM d_4-succinic acid, 100 mM NaCl, and 0.1 mM EDTA, pH 5.5, using a Centricon 3 ultrafiltration apparatus (Amicon). The substrates were dialyzed against water, lyophilized, and dissolved in a small volume of water. To obtain a 1:1 ribozyme−substrate complex, the concentrations of the ribozyme and the substrates were calculated from the absorbance at 260 nm using extinction coefficients of 271×10^3 cm^{-1} M^{-1} for the ribozyme and 109×10^3 cm^{-1} M^{-1} for the substrates (*24*). For each sample, ~40 μL of substrate was added to the NMR tube and the titration was monitored using the imino proton NMR spectrum. The concentrations of the NMR samples were 1.3 mM for the unlabeled and $^{13}C/^{15}N$-labeled R19:S19dA17, 1.2 mM for the unlabeled and $^{13}C/^{15}N$-labeled R19:S19dC, 1.0 mM for the unlabeled R19:S19dI, and 0.7 mM for the unlabeled R19:S19G17. The NMR samples were prepared in 90% H_2O/10% D_2O in 350 μL using 5 mm microcell NMR tubes (Shigemi Inc.) except for the unlabeled R19:S19dI sample which was in 550 μL in a standard 5 mm NMR tube. For studies of the ribozyme−substrate complexes in Mg^{2+}, the samples were extensively dialyzed by ultrafiltration against buffer containing 25 mM of d_4-succinic acid, 100 mM NaCl, pH 5.5, and 2.0 mM free $MgCl_2$, except for the $^{13}C/^{15}N$-R19:S19dA17 sample for which some spectra were also performed at 5.0 mM free Mg^{2+}. The NMR samples without Mg^{2+} ion were heated to 60 °C for 2 min and cooled on ice before each experiment to allow for complex formation, whereas the samples with Mg^{2+} ion were only heated to 30 °C before cooling on ice.

NMR Experiments. The 1D[1] proton and 2D NOESY spectra were acquired with an 11 echo sequence using pulsed-field gradients to suppress the water signal before the acquisition (*25*). The 11 echo delay was calculated to position the maximum of the excitation profile at 12.9 ppm. Isotope-edited NMR experiments were performed on the $^{13}C/^{15}N$-labeled hammerhead samples in the presence and absence of Mg^{2+}. The isotope-edited experiments can be acquired as isotope filtered or isotope selected in either the indirect (ω_1) or acquisition (ω_2) dimension, or as a combination of all four possible isotope-edited subspectra (*26*).

To identify the resonances from the substrate, ω_2 ^{13}C-filtered NOESY and ω_2 ^{13}C-filtered TOCSY spectra were performed on the $^{15}N/^{13}C$-labeled R19:S19dA17 and the $^{15}N/^{13}C$-labeled R19:S19dC17 samples at 15 and 25 °C. The ω_2 ^{13}C filter consisted of a 90°-Δ-[180° (^1H), 180° (^{13}C)]-Δ sequence which was followed by a ^{13}C 90° pulse, and the full pulse sequence for the ω_2 ^{13}C-filtered NOESY experiment is given in Figure 1A in the Supporting Information. The ω_2 ^{13}C filter was put prior to detection in the TOCSY (50 ms DIPSI-2) experiment (*27*). The ω_2 ^{13}C filter eliminates the signals from protons bound to a ^{13}C nucleus by creating unobservable heteronuclear multiple-quantum coherence (*28*, *29*). The phase of the last ^{13}C 90° pulse was cycled to suppress any residual ^{13}C coherences. Experiments were performed with and without ^{13}C decoupling in the ω_1 dimension to allow the unambiguous identification of any residual peaks from a proton bound to a ^{13}C. Water suppression was achieved by a WATERGATE sequence

[1] Abbreviations: 1D, one-dimensional; 2D, two-dimensional; NOE, FID, free induction decay; nuclear Overhauser effect; NOESY, nuclear Overhauser effect spectroscopy; ppm, parts per million; TOCSY, total correlation spectroscopy.

using selective square pulses on the water signal (*30*). Since the time for the WATERGATE sequence was longer than the ω_2 ^{13}C filter, the two sequences were only partially concatenated (*31*). In this case, the delay Δ in the ω_2 ^{13}C filter and the selective WATERGATE 90° pulses were set to 1.56 and 1.94 ms, respectively. In the NOESY experiments, water flip-back was performed with a 2.0 ms Gaussian 90° water selective pulse immediately prior to the ω_2 ^{13}C filter (*32*). The ^{1}H 90° pulse at the beginning of the t_1 period was phase shifted by 45° to allow the water signal to relax efficiently back to the $+z$-axis through radiation damping during the NOESY mixing time. The mixing time was set to 180 or 200 ms in the ω_2 ^{13}C-filtered NOESY experiments except for the ^{15}N/^{13}C-labeled R19:S19dA17 sample where experiments were also performed at mixing times of 50, 80, and 140 ms.

To observe intermolecular (ribozyme−substrate) NOEs, ω_1 and ω_2 ^{13}C-edited NOESY experiments were performed on the ^{15}N/^{13}C-labeled R19:S19dA17 and the ^{15}N/^{13}C-labeled R19:S19dC17 samples. All four ω_1/ω_2 and ^{13}C-filtered/^{13}C-selected subspectra were obtained in a single experiment using a slight modification of the pulse sequence in ref *33*, where matching pulsed-field gradients were included in the ω_1/ω_2 ^{13}C-filtered/^{13}C-selected sequence. The ω_1 and ω_2 ^{13}C-editing was accomplished by a Δ-[180° (^{1}H), $90°_x$-$90°_{\pm x}$ (^{13}C)]-Δ sequence where Δ was 2.78 ms (see Figure 1B in the Supporting Information). The ω_1 and ω_2 ^{13}C-editing sequences were positioned after the first 90° ^{1}H pulse and prior to detection, respectively. The WATERGATE sequence (*30*) was used to suppress the water signal and was completely included in the ω_2 ^{13}C-editing pulse sequence. Water flip-back was achieved with a 2.12 ms Gaussian 90° selective pulse at the end of the 200 ms NOESY mixing time. These ^{13}C-edited NOESY experiments were recorded at 15 or 25 °C. All the spectra were performed on a Varian Unityplus 500 MHz spectrometer equipped with z-axis pulsed-field gradients. The NMR data were processed on a Silicon Graphics computer with the program FELIX 2.35 or 95.0 (Biosym Inc.).

Calculation of Hammerhead Models with Mutants at the Cleavage Site. Models of the cleavage-site region for various hammerhead substrate complexes were generated by restrained molecular dynamics starting from the X-ray structure of McKay and co-workers (*5*). Protons were added to the X-ray structure and the cytosine at the cleavage site was replaced by either a guanine or an adenine, using the program Insight 2.35 (Biosym Inc.). For all calculations the substrate contained deoxyribose sugars as in the X-ray structure (*5*) and for the calculations with an adenine at the cleavage site, the base of residue T16.1 was replaced by a U. The restrained molecular dynamics calculations were performed with the program Discover 95.0 (Biosym Inc.) using the standard Discover default parameters and the AMBER force field. The restrained molecular dynamics calculations were performed using force constants of $k_{NOE} = 20$ kcal mol^{-1} A^{-2} for the experimental NOEs and $k_{XRAY} = 1.0$ kcal mol^{-1} A^{-2} for the proton−proton distances extracted from the X-ray structure. An equilibration period of 0.8 ps at 500 K was followed by 1 ps of dynamics, using 1.0 fs steps. Next the temperature was linearly decreased to 200 K during a total period of 3.5 ps. After dynamics, 1000 steps of conjugate gradient minimization was performed. Eleven different structures were calculated with the same protocol, starting from the same structure but with different initial velocities of the atoms. To keep the structures as close to the X-ray structure as possible, all the proton−proton distances <5 Å were included as constraints (with ranges ± 0.5 Å) except for distances involving protons on residue 17 which were eliminated from the constraint list. For calculations on the R19:S19G17 complex, six distance constraints were introduced between G17 and C3 to ensure formation of the Watson−Crick base pair identified from the NMR data (see below). A hydrogen bond donor−acceptor distance constraint was included for each of the three hydrogen bonds in the G−C base pair, and three other constraints were included between the heavy atoms in each hydrogen bond (the hydrogen-bonding constraints had ranges of ±0.1 Å). The following NOE connectivities observed in the ^{13}C/^{15}N-labeled R19:S19dA17 complex in Mg^{2+} were used to generate NMR distance constraints for the structural calculations on this system and were input with ranges of 2.5−5.0 Å: H_6(U16.1)/H_8(dA17), $H_{1'}$(U16.1)/H_8(dA17), H_8(dA17)/H_8(G1.1), $H_{1'}$-(dA17)/H_8(G1.1), H_8(dA17)/H_5(U16.1), H_6(U16.1)/H_8(G16.2), H_6(U16.1)/$H_{1'}$(G16.2).

Table 1: Equilibrium Dissociation Constants (K_d) of the Hammerhead Ribozyme with Substrates Containing Various Nucleotides at the Cleavage Site[a]

substrate	K_d (nM)	substrate	K_d (nM)
S8C17	50[b]	S8dC17	350[c]
S8A17	57[b]	S8dA17	750[c]
S8G17	2[b]	S8dG17	20[c]
S8I17	13[c]	S8dI17	100[c]

[a] The binding constants are for the R8-S8N17 substrates at 25 °C. The sequence of the R8-S8 system is given in Figure 2 in ref *13*. [b] These binding affinities are from ref *13*. [c] The binding affinities were measured here by both native gel electrophoresis and competitive inhibition using conditions and procedures as previously described (*13*).

RESULTS

Assignment of the Imino Proton Resonances of the Hammerhead Complexes. 2D NOESY experiments in 90% H_2O were used to assign base pairs in helical regions by identification of short distances between imino protons or between imino protons and aromatic or sugar protons on neighboring residues (*34*−*36*). The initial assignments for the R19:S19 complexes were made in the absence of Mg^{2+}. The imino protons for stem I of R19:S19dA17 were readily assigned from the sequential imino proton to imino proton NOESY cross-peaks (Figure 2, Supporting Information). The chemical shifts for the imino protons in stem I (see Table 1, Supporting Information) are very similar to those for the highly related R13:Sd13 hammerhead that was previously assigned in the lab (*37*). For R19:S19dA17, the G1.1 imino proton resonance was assigned from the NOESY cross-peak to G1.2 (Figure 2, Supporting Information), but the G2.7 imino proton resonance was not observed due to fast exchange with water caused by fraying of this terminal base pair. For stem II and the loop, the assignments for R19:S19dA17 confirmed the previous ones for R13:Sd13 (*37*). The G16.2 and G16.3 imino proton resonances in stem II were assigned in the ^{15}N/^{13}C-labeled R19:S19dA17 complex from NOESY spectra performed without ^{15}N decoupling, which distinguished the imino proton resonances on the

substrate from those on the ribozyme. Complete assignment of the $H_{1'}$, H_5, H_6, and H_8 resonances for the S19dA17 substrate in the hammerhead complex were made using ω_2 ^{13}C-filtered NOESY and ω_2 ^{13}C-filtered TOCSY experiments as described below (see Table 2, Supporting Information) (*26*, *33*). The sequential $H_{1'}$ to G imino proton NOEs (*36*) were then used to assign the G16.2 and G16.3 imino proton resonances. The G15.4 and G16.5 imino proton resonances are not observed due to fraying at the end of stem III. The U16.1 imino proton resonance is not observed in the NMR spectra due to fast exchange with the water which is consistent with the X-ray structure where this proton is not involved in a H-bond (*5*, *6*). The R19:S19dA17 and R19:S19dC17 complexes were also studied in the presence of Mg^{2+}. For these systems, the presence of Mg^{2+} only affected the line width and not the chemical shifts of the imino proton resonances.

Figure 2 shows the imino proton to imino/aromatic proton regions of the NOESY spectrum of the R19:S19G17 complex. As compared with the R19:S19dA17 complex, a new imino proton resonance is observed at 12.54 ppm, and this chemical shift is consistent with a G imino proton in a Watson−Crick G−C base pair (*35*). This imino proton resonance is assigned to G17 by observation of a cross-peak with the imino proton resonance for G1.1 (the arrow in Figure 2). The assignments were confirmed by analysis of the imino proton to aromatic proton regions of the NOESY spectra on the R19:S19dA17, R19:S19dC17, R19:S19G17, and R19:S19dI17 complexes (see Figure 3 in Supporting Information). The imino proton resonance assignments in the absence of Mg^{2+} for all the complexes studied here are given in Table 1 in Supporting Information.

To study the effect of the Mg^{2+} on G17−C3 base pairing, spectra were obtained on the R19:S19G17 complex in the presence of 2.0 mM $MgCl_2$. The cleavage is very slow for this substrate under the conditions used here, and the absence of a 2′,3′ cyclic phosphate peak in the 1D ^{31}P spectrum performed at the end of this study confirmed that the S19G17 substrate was not cleaved (data not shown). The presence of Mg^{2+} does not significantly affect the 1D imino proton region of the hammerhead complex, except for a broadening of the resonances (see Figure 4 in Supporting Information) (*37*, *38*). All the imino protons assigned for R19:S19G17 in Mg^{2+} had the same chemical shifts as they did in the absence of Mg^{2+}.

Resonance Assignment of the Nonexchangeable Protons of Substrates in the Hammerhead Complexes. Heteronuclear isotope-edited experiments were used to separate resonances in the S19dA17 and S19dC17 substrates from those in the ^{15}N/^{13}C-labeled R19 ribozyme. Assignment of the substrate resonances was obtained using ω_2 ^{13}C-filtered TOCSY and ω_2 ^{13}C-filtered NOESY experiments which suppress the aromatic and aliphatic proton signals on the ^{15}N/^{13}C-labeled R19 (*26*). Figure 3 shows a region of the ω_2 ^{13}C-filtered NOESY performed on the ^{15}N/^{13}C-labeled R19:S19dA17 sample in the absence and presence of 5.0 mM free Mg^{2+}. Resonance assignments were obtained using the sequential walk observed in the H_6, H_8/$H_{1'}$ region as shown in Figure 3A. This pathway is formed by the sequential connectivities between the sugar $H_{1'}$ on residue i and the base H_6/H_8 of residue $i - 1$ (*34*, *35*). Assignment of the resonances for the deoxynucleotide at the cleavage site was confirmed by

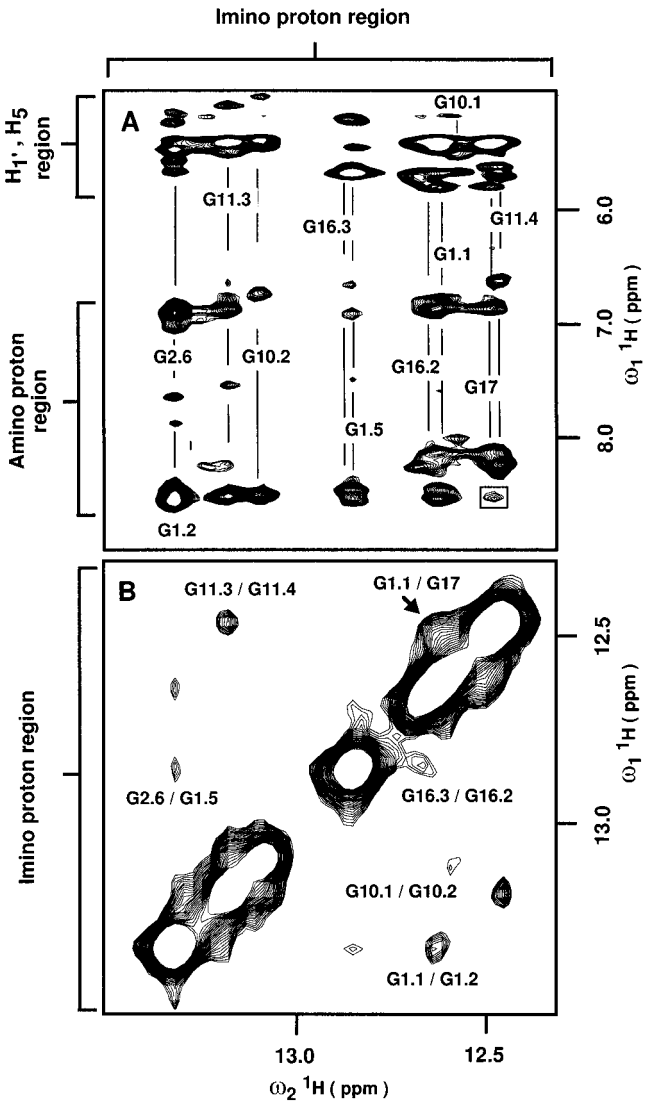

FIGURE 2: (A) Part of the imino proton to aromatic proton region, and (B) the imino proton to imino proton region of the 2D NOESY spectrum of the R19:S19G17 sample in H_2O recorded at 5 °C. The G17 imino proton at 12.54 ppm gives NOEs to the G1.1 imino proton (indicated by the arrow), and one of the amino protons on C2.1 (indicated by a box in panel A). The 2D NOESY spectrum was acquired in 80 h with a resolution of 39 Hz/point in t_1, 19 Hz/point in t_2, 450 transients, a recovery time of 1 s and a mixing time of 250 ms. The R19:S19G17 sample was prepared in buffer containing 25 mM d_4-succinate, 100 mM NaCl, pH 5.5, and does not contain Mg^{2+}.

the presence of connectivities with the $H_{2'}$ and $H_{2''}$ resonances at their characteristic chemical shifts. The H_5−H_6 connectivities in pyrimidines were assigned from the ω_2 ^{13}C-filtered TOCSY experiments. Sharper line widths were observed for the spectra recorded in absence of Mg^{2+} (Figure 3). Thus, the assignments were first made in absence of Mg^{2+} and these aided in assignments of the spectra with Mg^{2+} (Table 2 in Supporting Information). For the R19:S19dA17 sample in the presence and in absence of Mg^{2+}, all the substrate nucleotides were assigned in the $H_{1'}$ to H_8/H_6 sequential walk. For the R19:S19dC17 complex, all substrate residues except G1.1 were assigned. The H_8 and $H_{1'}$ resonances for G1.1 may overlap with other protons or may have broad line widths due to motion of this nucleotide. However, the imino proton of the G1.1 was assigned, confirming the formation of a stable G1.1−C2.1 Watson−Crick base pair.

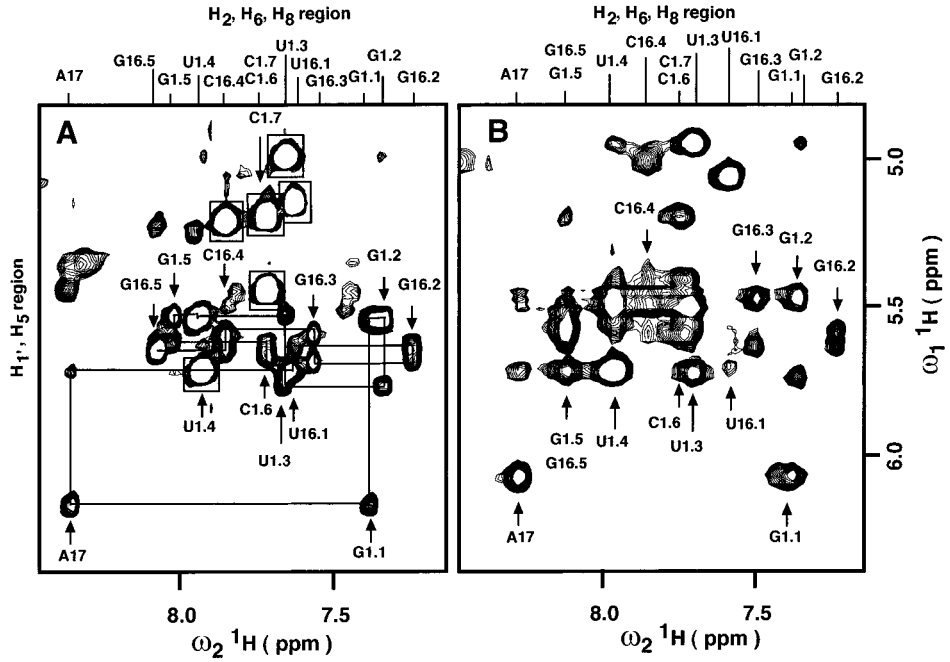

FIGURE 3: Regions of the ω_2 ^{13}C-filtered 2D NOESY experiments (*26*, *33*) performed on the ^{13}C/^{15}N-labeled R19:S19dA17 complex at 25 °C. In these experiments, resonances corresponding to a proton bonded to a ^{13}C nucleus are suppressed along the ω_2 dimension. (A) The experiment was performed on the ^{13}C/^{15}N-labeled R19 ribozyme in the complex with the unlabeled substrate S19dA17 in 90% H_2O/10% D_2O solution (no Mg^{2+}). (B) The same experiment was performed on this hammerhead sample but in the presence of 5.0 mM Mg^{2+}. The substrate assignments were obtained using the aromatic H_6/H_8 to $H_{1'}$ NOE pathway as shown in panel A. Boxed peaks were observed in the ω_1 ^{13}C-filtered 2D TOCSY experiment and correspond to the H_5/H_6 correlations. Both spectra were acquired with a resolution of 31 Hz/point in t_1, 12 Hz/point in t_2, a recovery time of 1 s and a NOESY mixing time of 180 ms. The spectrum in panel A was acquired in 36 h with 192 transients, and spectrum in panel B was acquired in 18 h with 96 transients.

NOE Connectivities between Protons in the Substrate. The ω_2 ^{13}C-filtered NOESY experiments were performed on the ^{13}C/^{15}N-labeled R19:S19dA17 and the ^{13}C/^{15}N-labeled R19:S19dC17 samples in 2.0 mM Mg^{2+} (see Figure 4). These spectra were used to extract NOE connectivities between protons on the substrate, because all the aromatic and aliphatic proton resonances from the ^{13}C/^{15}N-labeled R19 are eliminated along the ω_2 dimension. The same information is also present in the ω_1 ^{13}C-filtered/ω_2 ^{13}C-filtered NOESY spectrum (not shown), but the sensitivity of this experiment is reduced due to the longer delay used during the two filtering periods, compared to the ω_2 ^{13}C-filtered NOESY spectrum (see Figure 1 in Supporting Information). The H_8/H_6 to $H_{1'}$ region shows all the expected sequential NOE in the two stems for the both samples. For the ^{13}C/^{15}N-labeled R19:S19dA17 complex, NOEs were also observed between H_6(U16.1)/H_8(dA17), $H_{1'}$(U16.1)/H_8(dA17), H_8(dA17)/H_8-(G1.1), $H_{1'}$(dA17)/H_8(G1.1), and $H_{2',2''}$(dA17)/H_8(G1.1), which demonstrates that the dA17 at the cleavage site has short proton−proton distances to its two sequential neighbors. These NOEs were observed in the absence and presence of Mg^{2+} (see Figure 3). As discussed below, these U16.1 to dA17 NOEs are not predicted from the X-ray structures of the hammerhead. Thus, to confirm these NOE assignments, experiments were also performed without ^{13}C decoupling in the ω_1 and ω_2 dimensions. In absence of ^{13}C decoupling, all the peaks involving an aliphatic or an aromatic proton of the ^{13}C/^{15}N-labeled R19 are readily identified because they change from a singlet to a doublet. To test that these NOEs are not due to spin diffusion, experiments were performed with NOESY mixing times of 50, 80, 140, and 180 ms on the R19:S19dA17 sample in Mg^{2+}. The linearity of the NOE build-up curves indicate that these peaks arise from direct NOE transfer and not from spin diffusion. For the ^{13}C/^{15}N-labeled R19:S19dC17 sample in Mg^{2+}, no NOEs were observed between the nucleotide dC17 and its neighbors (Figure 4). The absence of connectivities between the aromatic protons of dC17 and G1.1 could be explained by resonance overlap of these protons. However, the NOE connectivities between $H_{1'}$ and H_6 of U16.1 and H_6 of dC17, would resonate in a well-resolved region and no NOEs are observed in the NOESY spectra.

Intermolecular NOE Connectivities. The ω_1/ω_2, ^{13}C-selected/^{13}C-filtered experiments were performed on the ^{13}C/^{15}N-labeled R19:S19dA17 and the ^{13}C/^{15}N-labeled R19:S19dC17 samples to identify intermolecular NOEs between the labeled ribozyme and the unlabeled substrate. In this experiment, addition or subtraction of the different FIDs give four subspectra from which the proton signal bound to a ^{13}C is selected or filtered along each dimension (*26*). Figure 5 shows the aromatic proton to $H_{1'}$ region of two of the four subspectra obtained from the ω_1/ω_2 ^{13}C-selected/^{13}C-filtered experiment on the ^{13}C/^{15}N-labeled R19:S19dC17 sample in 2.0 mM Mg^{2+}. Figure 5A is the ω_1 ^{13}C-filtered/ω_2 ^{13}C-filtered subspectra where the sensitivity allows observation of NOEs for protons that are separated by ∼4−4.5 Å. Since the sensitivity is the same for all four subspectra, any short (<4.0 Å) intermolecular proton−proton connectivities should be observed in the ω_1 ^{13}C-filtered/ω_2 ^{13}C-selected subspectra shown in Figure 5B. Only one intermolecular NOE is observed in this region, and none of the NOEs observed in this spectrum involve nonexchangeable protons on nucleotides U16.1 or dC17. The same experiment was performed on the ^{13}C/^{15}N-labeled R19:S19dA17 in Mg^{2+} (not shown), and again, no nonexchangeable protons on dA17 and U16.1 give NOEs to the R19 ribozyme.

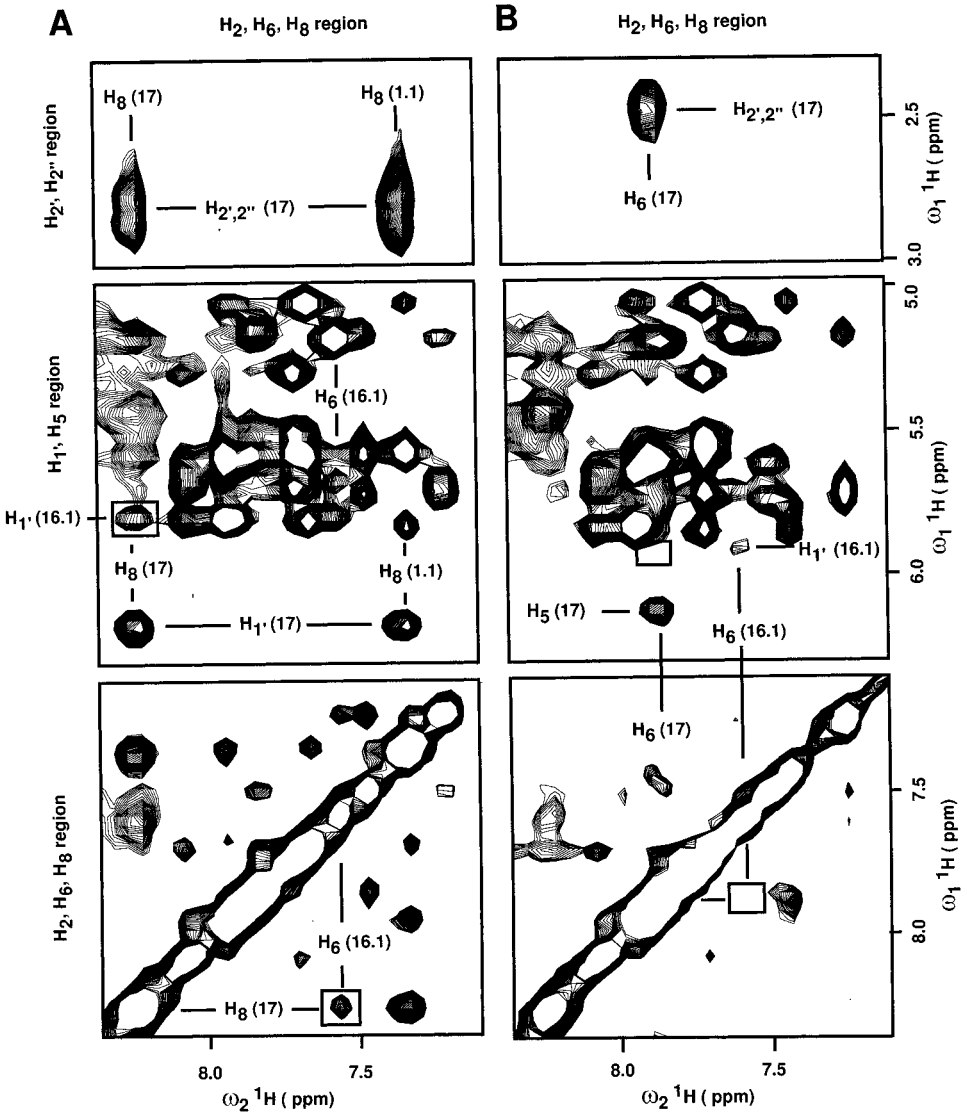

FIGURE 4: Three regions of the ω_2 ^{13}C-filtered 2D NOESY experiments performed at 25 °C, 2.0 mM Mg^{2+}. Spectra of the (A) $^{13}C/^{15}N$-labeled R19:S19dA17 and (B) $^{13}C/^{15}N$-labeled R19:S19dC17 complexes. The region on the bottom contains the $H_2/H_6/H_8$ to $H_2/H_6/H_8$ correlations. The region in the center contains $H_2/H_6/H_8$ to H_1'/H_5 correlations and the region on the top contains $H_2/H_6/H_8$ to $H_{2'}/H_{2''}$ correlations. In panel A, the boxed peaks indicate the NOEs observed between the aromatic and sugar protons on dA17 and protons on U16.1. The same connectivities should appear in the boxes displayed in panel B for the R19:S19dC complex. No NOEs were observed between U16.1 and dC17 in this spectrum. For the R19:S19dA17 complex in panel A, NOEs are observed between dC17 $H_{2'}/H_{2''}$ resonances and the G1.1 and dC17 H_8 resonances (top panel). For R19:S19dC17 in panel B NOEs were not observed between dC17 $H_{2'}/H_{2''}$ and G1.1 because the G1.1 H_8 was not unambiguously assigned. Both spectra were acquired in 48 h with 256 transients, at 31 Hz/point resolution in t_1, 12 Hz/point in t_2, a recovery time of 1 s and a mixing time of 200 ms.

NMR Studies of the Hammerhead with rG or dI at the Cleavage Site. 1D and NOESY spectra were performed on the R19:S19G17 complex in H_2O to test for formation of the G17−C3 base pair. Figure 2B shows an NOE cross-peak between the imino proton resonances of G1.1 and G17, indicating base pair formation, and the chemical shift of the G1.1 imino proton resonance is also consistent with a G−C Watson−Crick base pair. This conclusion is confirmed by the presence of two strong NOESY cross-peaks between G17 and two amino protons which are tentatively assigned to C3. In addition, the G17 imino proton gives a weak cross-peak with another resonance at 8.4 ppm which arises from a sequential NOE to the H-bonded amino proton on the neighboring base pair (C2.1) (Figure 2A). Together these results demonstrate formation of the C3−G17 base pair in the R19:S19G17 complex. NMR data were also obtained on the R19:S19dI17 complex that has a inosine at the cleavage site. Since no inosine imino proton resonance was observed in the NOESY spectra (Figure 3D, Supporting Information), there is no direct evidence for formation of a dI17-C3 base pair. Inosine lacks the amino group at C2 but should still be able to form an I17-C3 base-pair with two hydrogen bonds. The absence of the I17 imino proton resonance means that this proton is in fast exchange with water, indicating that this base pair is either not formed or fraying in the hammerhead complex.

K_d Measurements on the Hammerhead Complexes. The presence of the deoxyribose sugar at N17 in the S19dA17, S19dC17, and S19dI17 substrates makes it impossible for the hammerhead to cleave these molecules. To test for how the deoxyribose affects the stability of the ribozyme−substrate complex, the dissociation constants for substrates containing dA17, dC17, dI17, dG17, and rG17 at the cleavage site were measured by both native gel shift assays

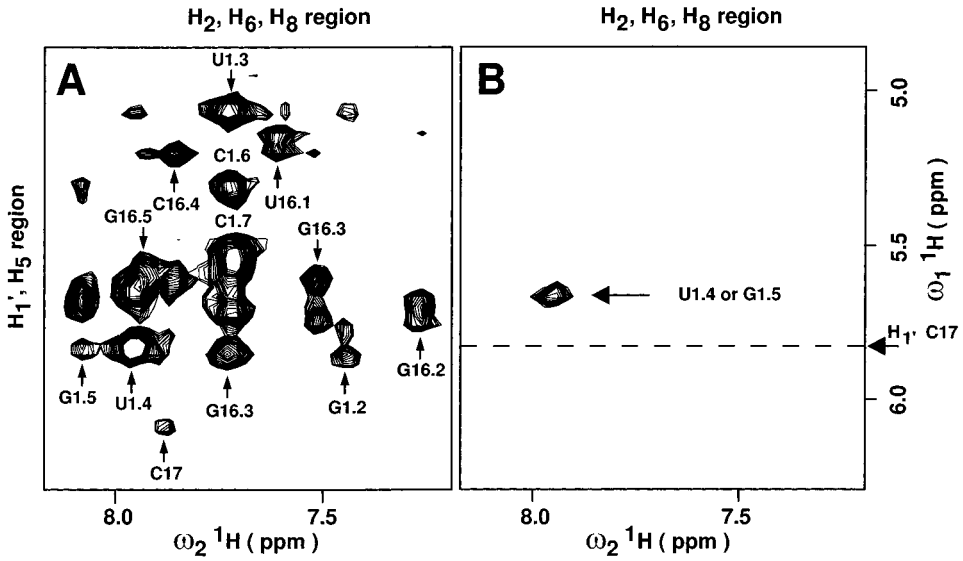

FIGURE 5: The $H_5/H_{1'}$ to $H_2/H_6/H_8$ region of the ω_1/ω_2 ^{13}C-filtered/^{13}C-selected NOESY experiment (*26*, *33*) performed on the $^{13}C/^{15}N$-labeled R19:S19dC17 complex at 25 °C in 2.0 mM Mg^{2+}. (A) The ω_1 ^{13}C-filtered/ω_2 ^{13}C-filtered subspectrum where only NOEs between two protons on the substrate are observed. The assignments for the substrate resonances were obtained as described in the text. (B) The ω_1 ^{13}C-filtered/ $\omega_2$$^{13}C$-selected subspectrum plotted at the same threshold level as in (A). This subspectrum contains NOEs between the $^{13}C/^{15}N$-labeled ribozyme and the substrate S19dC17. In this region, only one NOE is observed between the $H_{1'}$ of U1.4 or G1.5 in the S19dC17 substrate and an aromatic proton of the R19 ribozyme (at 7.94 ppm). The dashed line at 5.83 ppm indicates the ω_1 chemical shift of the $H_{1'}$ resonance of C17. None of the NOEs expected from the X-ray structure between residues dC17 and U16.1 of the substrate and protons in the ribozyme are observed (see text). The strong NOEs for the H_6 of dC17 in panel A demonstrate the high sensitivity of the experiment. This isotope-edited NOESY experiment was performed in 24 h, with 128 transients, at 31 Hz/point resolution in t_1, 12 Hz/point in t_2, a recovery time of 1 s and a mixing time of 200 ms.

and competitive inhibition, as previously described (*13*). The high stability of stems I and II in the R19:S19 complex makes it difficult to determine accurate binding constants in this system; therefore, the binding affinities were measured on the HH8 hammerhead complex that has shorter helical regions in stem I and stem III (*13*). Table 1 lists the binding constants for the substrates containing different deoxyresidues at the cleavage site measured here, along with the previously determined binding constants for substrates containing ribose sugars at the cleavage site (*13*). The binding affinities for the ribozyme−substrate complexes with a deoxyribose sugars at the cleavage site are 2.5−10-fold weaker than the same substrate with a ribose sugar at the cleavage site. Thus, there is a trend that the deoxyribose slightly destabilizes the ribozyme−substrate complex. However, the order of stability of the cleavage-site variants is the same in the ribose as the deoxyribose sugars (*13*). Thus, we would expect that the differences in kinetic and thermodynamic parameters measured in the cleavage-site variants with ribose substrates (*13*) also applies to the NMR complexes studied here.

DISCUSSION

Modeling Formation of the G17−C3 Base Pair in an Inactive Hammerhead. When the NMR spectra of the hammerhead R19:S19G17 complex are compared with spectra from complexes with other substrates (the S19dA17, S19dC17, or S19dI17 complexes in Figure 3 in Supporting Information), a new imino proton resonance is observed only for the hammerhead complex with a G at the cleavage site. This resonance was observed for R19:S19G17 complex in the absence and presence of 2.0 mM Mg^{2+} (Figure 4, Supporting Information). The observed NOEs and chemical shifts are consistent with formation of a Watson−Crick base pair between G17 and C3 in an A-form helical geometry (*35*). In both X-ray structures of the hammerhead (*5*, *6*), the amino proton of C17 at the cleavage site forms an H-bond with the N3 of C3 (Figure 6A). Restrained molecular dynamics calculations were used to determine what changes are required in the catalytic core to form a G17−C3 base pair. Distance constraints were introduced corresponding to a Watson−Crick G17−C3 base pair, and a representative model is shown in Figure 6B. Comparison with the initial X-ray structure demonstrates that this G17−C3 base pair can form with relatively minor changes from the X-ray structure, and in this model, only the backbone around G17 and C3 is significantly changed. This backbone conformational change is required to eliminate steric repulsion between C3 and G17, when the larger guanine base replaces the cytosine. In addition, comparison of the NOE data on the R19:S19G17 hammerhead complex (Figure 4, Supporting Information) indicates that there is little significant conformational difference of the G17−C3 base pair in the absence or presence of 2.0 mM Mg^{2+}.

Modeling the Conformation of the Cleavage Site in the R19:S19dA17 Complex. As discussed above, the isotope-edited NOESY spectra on the $^{13}C/^{15}N$-labeled R19:S19dA17 complex showed strong intrastrand sequential NOEs for the dA at the cleavage site that were not observed in the complex with a dC at the cleavage site (Figure 4). This indicates that there are differences in the structure and/or dynamics at the active site depending upon whether there is an A or C at the cleavage site. Restrained molecular dynamics calculations were performed to model to what extent the conformation of the X-ray structure has to change to be consistent with the observed NMR data. The goal of these calculations was to produce a model as similar as possible to the X-ray structure while still being consistent with the NOE data on the hammerhead complex with the dA at the cleavage site.

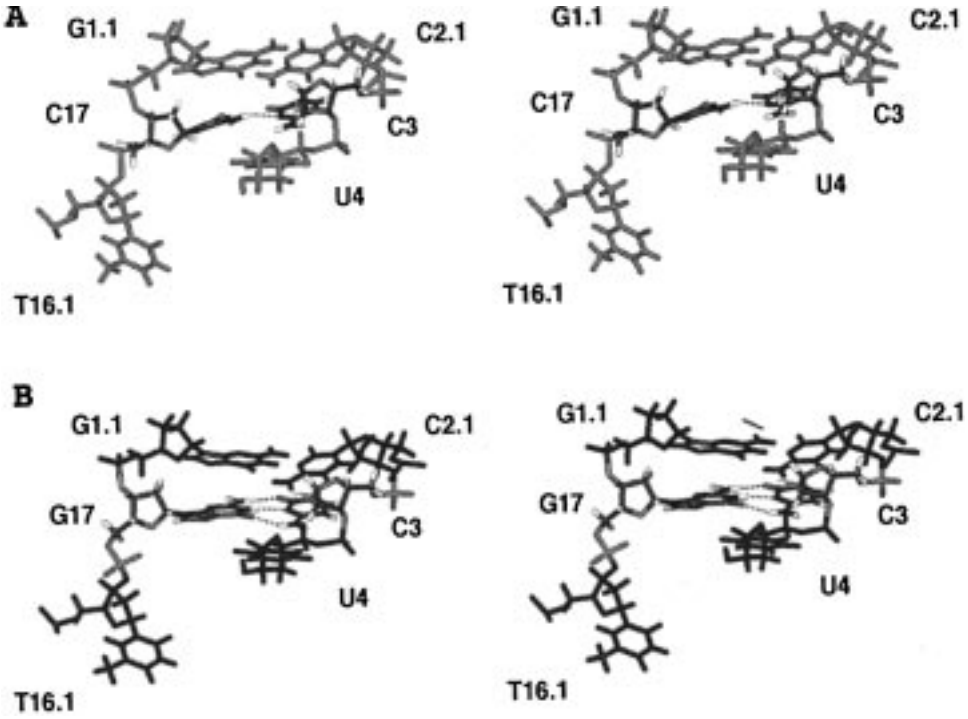

FIGURE 6: Stereoview of the active site of (A) the X-ray structure of the hammerhead by Pley et al. (*5*) and (B) the model calculation for formation of a Watson−Crick base pair between the G17 and the C3. Residues 3 and 17 are colored by atom types.

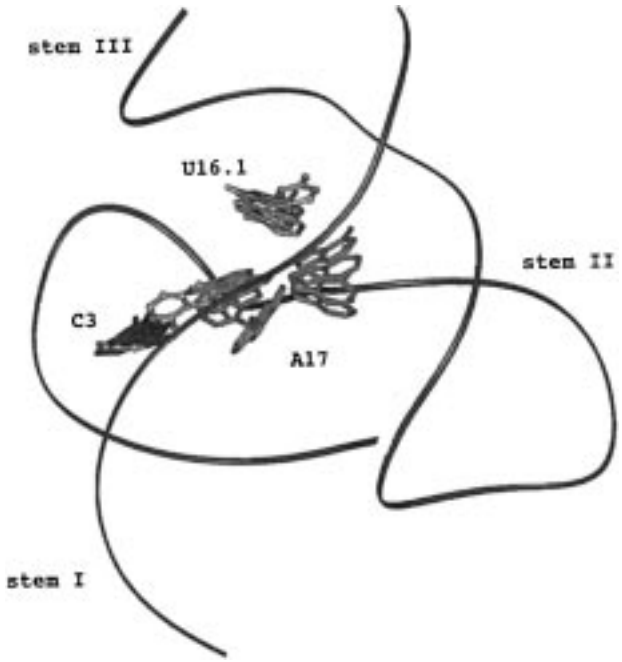

FIGURE 7: Models calculated from the X-ray structure using the experimental NOEs observed at the cleavage site. The structure colored in gold corresponds to the energy minimized X-ray structure where the nucleotide T16.1 and C17 were replaced by a uridine and an adenine, respectively. The other structures were generated by restrained molecular dynamics calculations to be as similar as possible to the X-ray structure while still fitting the experimental NMR data (see text). The purple ribbon traces the phosphate backbone for the initial structure. Only the bases of residues C3, A17, and U16.1 are shown and they are colored green, red and gray, respectively.

Figure 7 shows a superposition of 11 models that are all consistent with the experimental NOE data (the starting model is shown in gold). As illustrated in this figure, there are a number of ways by which the X-ray structure can be modified to be consistent with the NMR data, and dA at the cleavage site has the largest variation in these models. Figure 8A shows some of the experimental NOE constraints involving dA17 in the starting structure for the calculations. It is clear that the U16.1 to dA17 distances in the X-ray structure are too long to be observed in the NOESY spectra recorded here (distances of 5.6 and 8.5 Å), respectively. The calculations were thus performed to constraint these distances to be consistent with the experimental NOEs (between 2.5 and 5.0 Å). As seen in Figures 7 and 8, panels B and C, there are multiple structures that satisfy these constraints, with these structures falling into two families. Figure 8B shows an example from one family where the bases of U16.1 and dA17 move closer together. Thus, one way to satisfy the NOE data is with the base of U16.1 stacking on dA17, which is a different stacking pattern than what is observed in the X-ray structures where the bases of U16.1 and dA17 are splayed apart (*5*, *6*).

The calculations produced a second family of structures, one example of which is shown in Figure 8C. In this case, the experimental NOEs were satisfied by bringing together the base of U16.1 and A17 but by also changing the glycosidic angle of A17 from anti to syn. A syn conformation has a very short $H_{1'}$ to H_8 intraresidue distance (~2.5 Å) which should give rise to a large NOE (similar in size to the pyrimidine H_5-H_6 NOEs) (*35*). The A17 $H_{1'}$ to H_8 NOE is much smaller than the H_5-H_6 NOEs (Figure 4A) and therefore is not consistent with a true syn conformation. Thus, the family of models having a syn glycosidic angle for A17 is not compatible with the experimental NOEs (assuming a single static conformation for these residues). However, these NMR data would be consistent with a model where the A17 at the cleavage site is in equilibrium between a syn and anti conformation and the exchange lifetime between these conformations is fast on the NMR chemical shift time

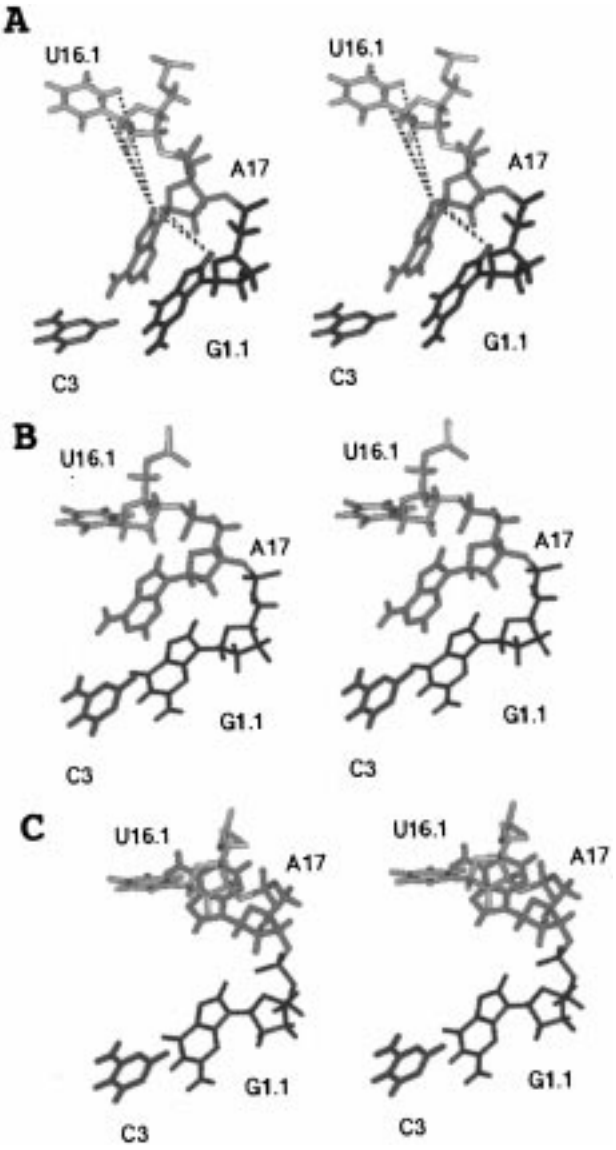

FIGURE 8: Cleavage site region for several of the structures shown in Figure 7. (A) The starting structure, which was obtained by energy minimization of the X-ray structure after replacing the nucleotides T16.1 and C17 by a uridine and an adenine, respectively. The black dotted lines correspond to the NOEs observed between residues A17 and the U16.1, in the $^{13}C/^{15}N$-labeled R19:S19dA17 complex. The structures shown in panels B and C are representative of the two different families, where A17 is in a anti and syn conformation, respectively (see text). Both of these structures are in agreement with the experimental NOEs observed at the cleavage site.

scale (lifetimes less than 1 ms). The conclusion from these data is that there is a significant change in the solution conformation of the hammerhead with a dA at the cleavage as compared with the X-ray structure of the hammerhead with dC or 2′O-methyl-C at the cleavage site.

It was rather surprising to find a difference in conformation between the X-ray structures of the hammerhead with a C at the cleavage site and the NMR models of the hammerhead with an A at the cleavage site. To determine if this difference was caused by a having a different nucleotide at the cleavage site, a sample of the $^{13}C/^{15}N$-labeled R19 complexed with a substrate containing a dC at the cleavage site was also studied. The ω_2 ^{13}C-filtered NOESY spectra on this complex are shown in Figure 4B. No interresidue U16.1 to C17 NOEs are observed in this spectrum. The boxes in the figure indicate the positions of potential H_6(U16.1)/H_6(dC17) and $H_{1'}$(U16.1)/H_6(dC17) NOEs, and there are clearly no cross-peaks for these connectivities. The strong U16.1 to dA17 interresidue NOEs that were observed in the hammerhead with the S19dA17 substrate are absent in the complex with the S19dC17 substrate. Thus, for the R19:S19dC17 complex the observed NMR data are consistent with the substrate conformation in the X-ray structures.

Conformation and Dynamics of the Active Site in the Hammerhead Ribozyme. To further address how consistent the solution NMR data are with the X-ray structures of the hammerhead, we calculated all short (<4 Å) intermolecular distances between protons on the ribozyme and protons on the substrate in the X-ray structure. Figure 9 shows the cleave-site region of the X-ray structure of the hammerhead (*5*) where some of the short (<4.0 Å) intermolecular proton−proton distances are illustrated. Having an isotopically labeled ribozyme complexed with an unlabeled substrate provides an ideal system for identifying short intermolecular proton−proton distances, through application of isotope-edited NOESY experiments. Figure 5B shows part of the ω_1 ^{13}C-selected/ω_2 ^{13}C-filtered NOESY subspectrum of the $^{13}C/^{15}N$-labeled R19:S19dC17 complex, where only intermolecular ribozyme−substrate NOEs are observed. Although complete assignments for the catalytic core of the hammerhead are not yet available, the only intermolecular NOE observed in this region of the spectrum is from a ribozyme aromatic proton to the $H_{1'}$ of U1.4 or G1.5. This cross-peak arises from an intermolecular interaction in stem I and does not involve the catalytic core of the hammerhead. However, this cross-peak has high signal-to-noise ratio, which is important in interpreting the absence of NOEs in this spectrum. The C17 $H_{1'}$ to A6 H_8 distance is highlighted with the green dashed line in Figure 9 because it should give rise to an NOE cross-peak at the C17 $H_{1'}$ chemical shift indicated in Figure 5B. No intermolecular NOE was observed at this chemical shift, even though the corresponding distance is 3.6 Å in the X-ray structure (Figure 9). The two shortest proton−proton distances between the substrate and catalytic core of the hammerhead in the X-ray structure are 2.2 and 2.4 Å for the T/U16.1 $H_{1'}$ to A6 $H_{1'}$ and the C17 H_6 to A6 $H_{2'}$ connectivities, respectively (*5*). Neither of these NOEs are present in the appropriate regions of the ω_1 ^{13}C-filtered/ω_2 ^{13}C-selected subspectrum of Figure 5B. This lack of NOEs could result from (1) the conformation of cleavage-site region being different under the NMR solution conditions as compared with the X-ray crystal structure conditions, or (2) part of the U-turn region in active site of the hammerhead being more dynamic than the substrate residues at the cleavage site. The absence of NOEs thus arises from too-long distances or from flexibility that reduces the intensity of the NOE. Analysis of the ω_1 ^{13}C-filtered/ω_2 ^{13}C-selected spectra on the $^{13}C/^{15}N$-labeled R19:S19dA17 complex also showed an absence of predicted ribozyme−substrate NOEs for the cleavage-site region (not shown).

Structure and Activity of Nucleotide Variants at the Cleavage Site of the Hammerhead Ribozyme. The catalytic activities for cleavage-site variants have been extensively studied in the hammerhead ribozyme (*2*, *7*−*13*, *39*). These studies have shown that the cleavage rate for having a rG at the cleavage site is down 1000−30000-fold in several

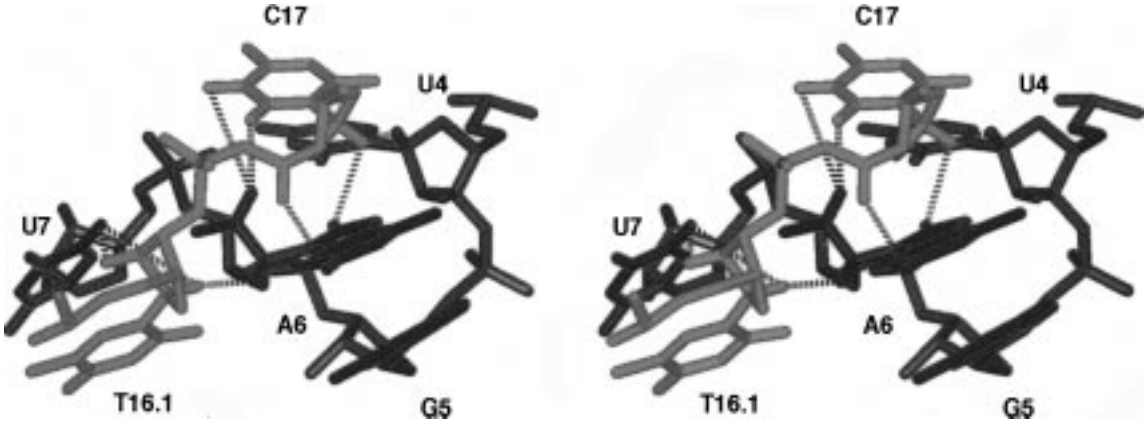

FIGURE 9: Stereoview of the cleavage site region of the X-ray structure of the hammerhead ribozyme. Residues in red belong to the substrate and the residues in purple are from the ribozyme. A variety of intermolecular (ribozyme−substrate) NOEs are expected for residues near the cleavage site, and the dashed lines correspond to some of these short (<4 Å) proton−proton distances. The green dash line corresponds to the C17 $H_{1'}$ to A6 H_8 distance (see the text). Only heavy atoms are shown except for the protons involved in the highlighted short proton−proton distances.

different hammerhead constructs, relative to having a rC at the cleavage site. In contrast, the cleavage rate for the other three natural nucleotides vary by less than a factor of 10. The reduced rate for rG was previously hypothesized to arise from formation of a G17−C3 base pair, which traps the hammerhead in an inactive conformation (*2, 10, 13, 19*). The NMR data obtained here provide direct evidence for formation of this base pair and therefore confirm that the rG17 substrate helps inhibit cleavage by stabilization of the ground-state ribozyme−substrate complex. The binding affinity of an rG17 substrate to the hammerhead ribozyme is 25−150 times tighter than the three other natural nucleotides (*13*). However, as previously discussed (*13*), the reduced k_{cat} for the cleavage of rG is not fully accounted for by stabilization of the ground-state ribozyme-rG17 substrate complex. The detailed kinetic analysis demonstrated that the transition state for the rG substrate was also substantially destabilized, leading to the >5000-fold lower cleavage rate than the rC17 or rA17 substrates (*13*).

NMR studies were also performed on the R19:S19dI17 complex to test for how loss of an H-bond donor in the inosine would affect formation of the base pair between residue 17 and C3. In this complex, the imino proton of the I17 was not observed due to fast exchange with solvent (see Figure 3 in Supporting Information), suggesting that the I17−C3 base pair is destabilized relative to the G17−C3 base pair. The K_d measurements also indicate that the I−C base pair is less stable than the G−C base pair (see Table 1).

The biochemical studies have also shown that the ribozyme−rA17 substrate complex is destabilized by 1 kcal/mol in both the ground state and the transition state as compared with the rC17 substrate (*13*). From these data, it was proposed that the A17 substrate might go through a different reaction pathway for cleavage than the C17 substrate (*13*). The NMR data on the ribozyme complexes with the dA17 and dC17 substrates demonstrate that there are significant differences in the structure and/or dynamics of the active site in these two complexes, therefore, supporting the hypothesis of a different reaction pathway. Several strong sequential U16.1 to dA17 NOEs observed for the R19:S19dA17 complex are not seen in the R19:S19dC17 complex (Figure 4). These NOEs arise from short proton−proton distances involving A17 that are not predicted from the X-ray structures of the hammerhead (*5, 6*). Figures 7 and 8 show model structures that are consistent with the observed NOEs involving dA17. These models clearly illustrate that the position of A16 must change relative to the X-ray structure and move closer to U16.1 to fit the experimental NMR data. Another important feature of the NMR studies is that for both the R19:S19dA17 and R19:S19dC17 complexes, short intermolecular proton−proton distances predicted in the X-ray structure are not observed in the NMR spectra (Figures 5 and 9). This means that there are either differences in the conformation of the cleavage site in the crystal and solution structures or unusual dynamics for the active-site residues in these complexes. For example, intermediate exchange on the NMR time scale (lifetimes of microseconds to milliseconds) can lead to predicted NOEs not being observed due to exchange broadening of individual resonances. It is not yet possible to determine if the observed differences between the NMR and X-ray structures are a result of conformation differences or flexibility at the active site of the hammerhead, and additional NMR studies of the hammerhead are being pursued to help understand these differences.

ACKNOWLEDGMENT

We wish to thank Arlene Hangar and Paul Michiels for help in preparation of the R19 ribozymes.

SUPPORTING INFORMATION AVAILABLE

Two tables of chemical shifts of the proton resonances and four figures of pulse sequences for NOESY and the proton region of the 2D NOESY spectra (8 pages). Ordering information is given on any current masthead page.

REFERENCES

1. Keese, P., and Symons, R. H. (1987) in *Viroids and Viroid-like Pathogens* (Semancik, J. S., Ed.) pp 1−47, CRC Press, Boca Raton.
2. Ruffner, D. E., Stormo, G. D., and Uhlenbeck, O. C. (1990) *Biochemistry 29*, 10695−10702.
3. Symons, R. H. (1989) *Trends Biochem. Sci. 14*, 445−450.
4. Dahm, S. C., Derrick, W. B., and Uhlenbeck, O. C. (1993) *Biochemistry 32*, 13040−13045.

5. Pley, H. W., Flaherty, K. M., and McKay, D. B. (1994) *Nature 372*, 68−74.
6. Scott, W. G., Finch, J. T., and Klug, A. (1995) *Cell 81*, 991−1002.
7. Koizumi, M., Iwai, S., and Ohtsuka, E. (1988) *FEBS Lett. 239*, 285−288.
8. Koizumi, M., Iwai, S., and Ohtsuka, E. (1988) *FEBS Lett. 228*, 228−230.
9. Koizumi, M., Hayase, Y., Iwai, S., Kamiya, H., Inoue, H., and Ohtsuka, E. (1989) *Nucleic Acids Res. 17*, 7059−7071.
10. Koizumi, M., and Ohtsuka, E. (1991) *Biochemistry 30*, 5145−5150.
11. Nakamaye, K. L., and Eckstein, F. (1994) *Biochemistry 33*, 1271−1277.
12. Shimayama, T., Nishikawa, S., and Taira, K. (1995) *Biochemistry 34*, 3649−3654.
13. Baidya, N., and Uhlenbeck, O. C. (1997) *Biochemistry 36*, 1108−1114.
14. van Tol, H., Buzayan, J. M., Feldstein, P. A., Eckstein, F., and Bruening, G. (1990) *Nucleic Acids Res. 18*, 1971−1975.
15. Slim, G., and Gait, M. J. (1991) *Nucleic Acids Res. 19*, 1183−1188.
16. Setlik, R. F., Shibata, M., Sarma, R. H., Sarma, M. H., Kazim, A. L., Ornstein, R. L., Tomasi, T. B., and Rein, R. (1995) *J. Biomol. Struct. Dyn. 13*, 515−522.
17. Scott, W. G., Murray, J. B., Arnold, J. R. P., Stoddard, B. L., and Klug, A. (1996) *Science 274*, 2065−2069.
18. Peracchi, A., Beigelman, L., Scott, E. C., Uhlenbeck, O. C., and Herschlag, D. (1997) *J. Biol. Chem. 272*, 26822−26826.
19. Perriman, R., Delves, A., and Gerlach, W. L. (1992) *Gene 113*, 157−163.
20. Beigelman, L., Karpeisky, A., Matulic-Adamic, J., Haeberli, P., Sweedler, D., and Usman, N. (1995) *Nucleic Acids Res. 23*, 4434−4442.
21. Wincott, F., DiRenzo, A., Shaffer, C., Grimm, S., Tracz, D., Workman, C., Sweedler, D., Gonzalez, C., Scaringe, S., and Usman, N. (1995) *Nucleic Acids Res. 23*, 2677−2684.
22. Milligan, J. F., Groebe, D. R., Witherell, G. W., and Uhlenbeck, O. C. (1987) *Nucleic Acids Res. 15*, 8783−8789.
23. Nikonowicz, E. P., Sirr, A., Legault, P., Jucker, F. M., Baer, L. M., and Pardi, A. (1992) *Nucleic Acids Res. 20*, 4507−4513.
24. Legault, P. (1995) Ph.D. Thesis, University of Colorado, Boulder.
25. Sklenár, V., and Bax, A. (1987) *J. Magn. Reson. 74*, 469−479.
26. Otting, G., and Wüthrich, K. (1990) *Q. Rev. Biophys. 23*, 39−96.
27. Davis, D. G., and Bax, A. (1985) *J. Am. Chem. Soc. 107*, 2820−2821.
28. Gemmecker, G., Olejniczak, E. T., and Fesik, S. W. (1992) *J. Magn. Reson. 96*, 199−204.
29. Vuister, G. W., Kim, S. J., Wu, C., and Bax, A. (1994) *J. Am. Chem. Soc. 116*, 9206−9210.
30. Piotto, M., Saudek, V., and Sklenár, V. (1992) *J. Biomol. NMR 2*, 661−665.
31. Simorre, J. P., Zimmermann, G. R., Pardi, A., Farmer, B. T., II, and Mueller, L. (1995) *J. Biomol. NMR 6*, 427−432.
32. Grzesiek, S., and Bax, A. (1993) *J. Am. Chem. Soc. 115*, 12593−12594.
33. Otting, G., and Wüthrich, K. (1989) *J. Magn. Reson. 85*, 586−594.
34. Wüthrich, K. (1986) *NMR of Proteins and Nucleic Acids*, John Wiley & Sons, New York.
35. Wijmenga, S. S., Mooren, M. M. W., and Hilbers, C. W. (1993) in *NMR of Macromolecules* (Roberts, G. C. K., Ed.) pp 217−288, Oxford University Press, Oxford.
36. Heus, H. A., and Pardi, A. (1991) *J. Am. Chem. Soc. 113*, 4360−4361.
37. Heus, H. A., and Pardi, A. (1991) *J. Mol. Biol. 217*, 113−124.
38. Simorre, J. P., Legault, P., Hangar, A. B., Michiels, P., and Pardi, A. (1997) *Biochemistry 36*, 518−525.
39. Baidya, N., Ammons, G. E., Matulic-Adamic, J., Karpeisky, A. M., Beigelman, L., and Uhlenbeck, O. C. (1997) *RNA*, 1135−1142.
40. Hertel, K. J., Pardi, A., Uhlenbeck, O. C., Koizumi, M., Ohtsuka, E., Uesugi, S., Cedergren, R., Eckstein, F., Gerlach, W. L., Hodgson, R., and Symons, R. H. (1992) *Nucleic Acids Res. 20*, 3252.

BI972493Z